Quantum Modeling of the Carrier Mobility in FDSOI Devices

Viet-Hung Nguyen, Yann-Michel Niquet, François Triozon, Ivan Duchemin, Olivier Nier, and Denis Rideau

***Abstract*— We compute the electron and hole mobilities in ultrathin body and buried oxide, fully depleted silicon on insulator devices with various high-κ metal gate-stacks using nonequilibrium Green's functions (NEGF). We compare our results with experimental data at different back gate biases and temperatures. That way, we are able to deembed the different contributions to the carrier mobility in the films (phonons, front and back interface roughness, and remote Coulomb scattering). We discuss the role played by each mechanism in the front and back interface inversion regimes. We draw attention, in particular, to the clear enhancement of electron- and hole–phonons interactions in the films. These results show that FDSOI devices are a foremost tool to sort out the different scattering mechanisms in Si devices, and that NEGF can provide valuable inputs to technology computer aided design.**

***Index Terms*— Carrier–phonon interactions, FDSOI devices, Green's functions, mobility.**

I. Introduction

ULTRA thin body and buried oxide (BOX), fully depleted silicon on insulator (UTBB-FDSOI) devices are very attractive alternatives to bulk CMOS for the 14-nm node and beyond [1]–[3]. Indeed, they afford tight electrostatic control and are very versatile. In particular, the substrate acts as an efficient back gate thanks to the thin BOX, which can be used to tune the threshold voltage and optimize the transport properties of the devices. It has notably been demonstrated that the carrier mobility can be significantly enhanced at high density in the reverse regime (back bias $V_{\rm bg} > 0$ for nFDSOI and $V_{\rm bg} < 0$ for pFDSOI devices) [4], [5].

The mobility in UTBB-FDSOI devices is actually limited by a complex interplay between carrier–phonons interactions [6], [7], front interface roughness (FSR) and back interface roughness (BSR) [8], [9], remote Coulomb scattering (RCS) [10]–[12], and possibly remote phonon scattering (RPS) [12], [13]. The strength of most of these mechanisms depends a lot on the applied front and back gate bias voltages. UTBB-FDSOI devices, therefore, appear as a foremost tool to investigate the impact of different scattering mechanisms on the transport properties of silicon thin films. However, deembedding the various contributions to the mobility is far from straightforward and requires the support from accurate models for the physics of these devices. Such a deembedding is also an essential step toward the design of efficient Technology Computer Aided Design (TCAD) models [14] that can speed-up and secure the development of FDSOI technologies.

For that purpose, we have developed a multibands $\mathbf{k}\cdot\mathbf{p}$ nonequilibrium Green's functions (NEGF) code able to deal with realistic, large scale structures [15], [16]. NEGF solvers are based on an explicit description of real space disorders, such as surface roughness and remote Coulomb charges, and deal with scattering nonperturbatively. They are, therefore, particularly well suited to the description of these mechanisms in quantum confined devices. Although expensive, NEGF has benefited from advances in numerical algorithms and from the increasing availability of supercomputers. We have recently setup a solid methodology for the calculation of carrier mobilities within the NEGF framework [16], and shown, in particular, that NEGF provides a more accurate description of surface roughness scattering than most models used in semiclassical Kubo–Greenwood (KG) solvers.

In this paper, we demonstrate that NEGF solvers are ready to address present (and future) technologies. Using NEGF calculations, we deembed the different contributions to the mobility measured on advanced n and pFDSOI devices. We discuss the physics and operation of these devices, and the role played by carrier–phonon interactions, surface roughness, and remote Coulomb scattering at different back gate voltages.

We introduce the devices and present the experimental data in Section II, then review our NEGF methodology in Section III, and discuss the deembedding strategy and results in Section IV.

II. Devices and Experimental Data

The devices have been processed on 300-nm (100) SOI wafers with an undoped, 7.5-nm-thick Si film on a 25-nm BOX [17]. The substrate below the BOX acts as a back gate. The front gate-stack is made of a 1.8-nm-thick HfSiON layer

Manuscript received May 20, 2014; revised June 26, 2014; accepted July 7, 2014. Date of publication July 29, 2014; date of current version August 19, 2014. This work was supported by the French National Research Agency through the Quasanova and Noodles Projects. The calculations were run on the TGCC/Curie machine using allocations from GENCI and PRACE. The review of this paper was arranged by Editor M. J. Kumar.

V.-H. Nguyen, Y.-M. Niquet, and I. Duchemin are with the Laboratoire de Simulation Atomistique, Institute for Nanosciences and Cryogenics, Université Grenoble Alpes, Grenoble 38054, France, and also with the Laboratoire de Simulation Atomistique, Institute for Nanosciences and Cryogenics, Commissariat à l'énergie Atomique et aux Énergies Alternatives, Grenoble 38054, France (e-mail: viet-hung.nguyen@u-psud.fr; yniquet@cea.fr; ivan.duchemin@cea.fr).

F. Triozon is with the Université Grenoble Alpes, Grenoble 38000, France, and also with the Laboratory for Electronics and Information Technology, Commissariat à l'énergie Atomique et aux Énergies Alternatives, Minatec, Grenoble 38000, France (e-mail: francois.triozon@cea.fr).

O. Nier and D. Rideau are with STMicroelectronics, Crolles 38920, France (e-mail: olivier.nier@st.com; denis.rideau@st.com).

Color versions of one or more of the figures in this paper are available online at http://ieeexplore.ieee.org.

Digital Object Identifier 10.1109/TED.2014.2337713

0018-9383 © 2014 IEEE. Personal use is permitted, but republication/redistribution requires IEEE permission.
See http://www.ieee.org/publications_standards/publications/rights/index.html for more information.

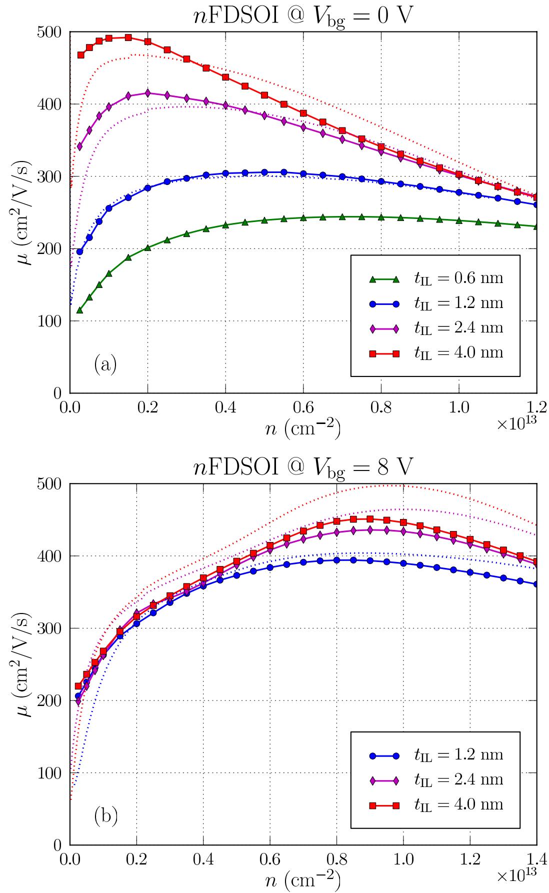

Fig. 1. Room-temperature electron mobility as a function of carrier density in nFDSOI devices with various ILs (see text), at back gate voltages (a) $V_{bg} = 0$ V and (b) $V_{bg} = 8$ V. The solid lines with symbols are the NEGF calculations, the dotted lines the experimental data.

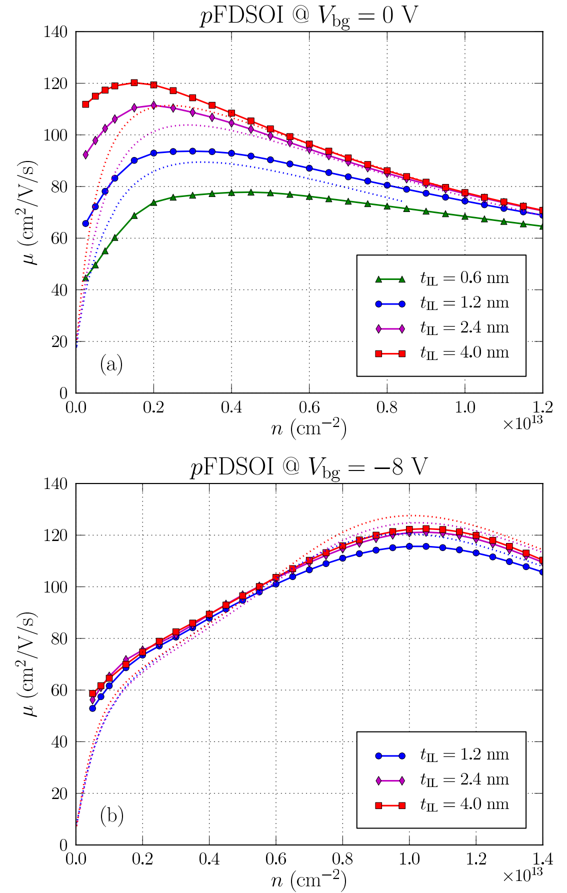

Fig. 2. Room-temperature hole mobility as a function of carrier density in pFDSOI devices, at back gate voltages (a) $V_{bg} = 0$ V and (b) $V_{bg} = -8$ V. The solid lines with symbols are the NEGF calculations, the dotted lines the experimental data.

on top of a SiON interfacial layer (IL) with thickness t_{IL} ranging from 1.2 to 4 nm. The electron and hole mobilities have been measured along [001] with a split CV method on $W = 0.9\ \mu$m $\times$ $L = 0.9\ \mu$m devices, and corrected from contact resistances $R_{acc} \approx 2 \times 60\ \Omega.\mu$m.

The electron and hole mobilities measured for three different ILs are plotted in Figs. 1 and 2, for back gate voltages $V_{bg} = 0$ V and $V_{bg} = \pm 8$ V. The carrier mobilities show a strong dependence on V_{bg} as the device switches from front to back interface inversion (at positive V_{bg} for electrons and negative V_{bg} for holes) [5]. In particular, the electron and hole mobility peak shifts from low-carrier density for $V_{bg} = 0$ V, to high-carrier density $n \approx 10^{13}$ cm^{-2} for $V_{bg} = \pm 8$ V. These data will be discussed in detail in Section IV.

The dielectric constants of the oxides have been obtained from the capacitance $C(V_{fg}, V_{bg})$ and threshold voltage $V_{th}(V_{bg})$ maps: $\varepsilon_{HfSiON} \approx 20$, $\varepsilon_{IL} = 5.2$ for $t_{IL} = 2.4$ nm and $t_{IL} = 4.0$ nm (oxide GO1), and $\varepsilon_{IL} = 6.6$ for $t_{IL} = 1.2$ nm (oxide GO2). GO1 and GO2 actually result from a different nitridation process.

III. NEGF Methodology

The carrier mobility has been computed with NEGF [18] along the lines of [16], on devices which are 20-nm wide and up to 90-nm long. The electron band structure is described with a nonparabolic two bands $\mathbf{k} \cdot \mathbf{p}$ model coupling opposite Δ valleys [19], and the hole band structure with a three bands $\mathbf{k} \cdot \mathbf{p}$ model (no spin–orbit coupling) [20]. We use a longitudinal mass $m_l^* = 0.916\, m_0$ and a transverse mass $m_t^* = 0.191\, m_0$ in Si, and an isotropic mass $m^* = 0.5\, m_0$ in SiO_2, with a barrier $\Delta V = 3.15$ eV at the interface. As for holes, we use Luttinger parameters $\gamma_1 = 4.270$, $\gamma_2 = 0.315$, and $\gamma_3 = 1.387$, and a barrier $\Delta V = -4.5$ eV at the Si/SiO_2 interface. The carriers can penetrate up to 1 nm in SiO_2. NEGF is based on an *explicit*, highly accurate real space description of disorder and screening (Fig. 3), and is able to deal with elastic (surface roughness and Coulomb) and carrier–phonon scattering nonperturbatively [16]. For electrons, we account for acoustic phonon scattering with an isotropic deformation potential $D_{ac} = 14.6$ eV, and for optical phonon scattering with the three f and the three g processes of [21]. This value of D_{ac} is significantly larger than in bulk ($D_{ac} = 9$ eV), but is widely accepted in thin films as it reproduces the universal mobility data much better [6] (also see Section IV). For holes, we use a diagonal hole–phonon interaction [7] with one single acoustic deformation potential Ξ_{ac} and one single optical deformation potential DK_{opt} ($\Xi_{ac} = 10.2$ eV and $DK_{opt} = 15$ eV/Å in bulk). We have also designed a nondiagonal model (featuring interband couplings), which does not, however, produce much different results. Surface roughness samples are generated from an exponential autocorrelation

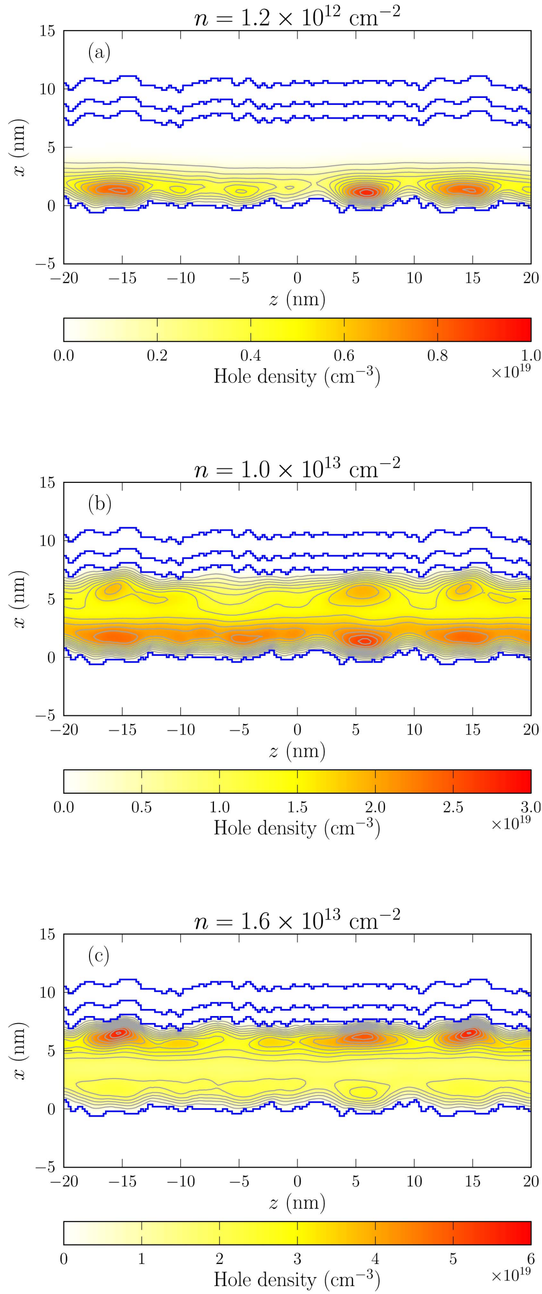

Fig. 3. NEGF hole density in the device at back gate voltage $V_{bg} = -8$ V, for sheet density n increasing from (a) to (c) ($t_{IL} = 1.2$ nm). The solid blue lines delimit, from top to bottom, the gate, the HfSiON and SiON layers, the Si film, and the BOX. The front gate-stack interfaces have been chosen conformal. Nonconformal interfaces slightly enhance scattering (remote surface scattering [24]). There is a transition from (a) back interface inversion at low density to (c) front interface inversion at high density.

function characterized by rms fluctuations Δ and correlation length Λ [8]. Remote Coulomb scattering is modeled by a distribution of positive charges at the HfSiON/SiON interface, with density n_{RCS}, as detailed in [16]. The NEGF equations are solved self-consistently on three transverse k_y points, in a fully coupled mode space approach [22], with up to 512 modes for the three bands $\mathbf{k} \cdot \mathbf{p}$ model [16], [23]. The back gate substrate is modeled as a doped semiconductor, treated semiclassically.

Simulations with carrier–phonons scattering only (which can be made on simpler test structures) suggest that the three bands $\mathbf{k} \cdot \mathbf{p}$ model overestimates the mobility by around 5% with respect to the six bands $\mathbf{k} \cdot \mathbf{p}$ model with spin–orbit coupling.

IV. Results and Discussion

We successively describe our deembedding strategy, the results for electrons, then for holes.

A. Deembedding Strategy

We have first computed reference mobilities for FSR (μ_{FSR}^{ref}), BSR (μ_{BSR}^{ref}), and RCS (μ_{RCS}^{ref}), assuming $n_{RCS} = n_{ref} = 5 \times 10^{13}$ cm^{-2}, and $\Delta = \Delta_{ref} = 0.47$ nm, $\Lambda = \Lambda_{ref} = 1.3$ nm at both interfaces [9]. These partial mobilities are defined with respect to the phonon-limited mobility μ_{PH} as

$$\mu_M^{-1} = \mu_{PH+M}^{-1} - \mu_{PH}^{-1} \quad (1)$$

where M is a given elastic mechanism (FSR, BSR, or RCS), and μ_{PH+M} is the NEGF mobility computed with only phonons and this mechanism enabled. As discussed in [16], including phonons (which are the only intrinsic source of scattering) in all simulations softens long-range interference effects in quantum transport calculations. Those mobilities also satisfy Matthiessen's rule much better than the usual, direct single mechanism calculations, even when RCS is strong [25]. Indeed, Matthiessen's rule is satisfied *by design* for μ_{PH} and μ_M, and holds reasonably well when two or more elastic mechanisms are concurrent [16].

Since the RCS mobility is expected to decrease as $1/n_{RCS}$ [10], [12], and the surface roughness mobility as $1/\Delta^2$ [8], [16], we might tentatively write the total mobility μ as

$$\mu^{-1} = \mu_{PH}^{-1} + \frac{n_{RCS}}{n_{ref}}(\mu_{RCS}^{ref})^{-1} + \left(\frac{\Delta_{FSR}}{\Delta_{ref}}\right)^2 (\mu_{FSR}^{ref})^{-1} + \left(\frac{\Delta_{BSR}}{\Delta_{ref}}\right)^2 (\mu_{BSR}^{ref})^{-1} \quad (2)$$

and deembed the different mechanisms by looking for the n_{RCS}, Δ_{FSR}, and Δ_{BSR} that best reproduce the experimental data. Note that surface roughness mobilities also depend on the correlation length Λ in a rather intricate way [26]; different (Δ, Λ) pairs can yield almost the same mobility curves, so that it is, practically, neither possible to assess Δ and Λ independently, nor to distinguish between exponential and Gaussian surface roughness autocorrelation profiles [8]. Yet the extracted surface roughness mobilities shall be accurate, even though the resulting Δ and Λ might not match the actual structure. In the following, we set $\Lambda = 1.3$ nm, which is a widely accepted value [8], [9], and fit Δ on the experiment.

B. Electrons

Such a procedure applied to the nFDSOI data collected for the different ILs and V_{bg}'s yields

$$\begin{aligned} n_{RCS} &= 3.5 \times 10^{13} \text{ cm}^{-2} \\ \Delta_{FSR} &= 0.37 \text{ nm} \\ \Delta_{BSR} &= 0.33 \text{ nm}. \end{aligned} \quad (3)$$

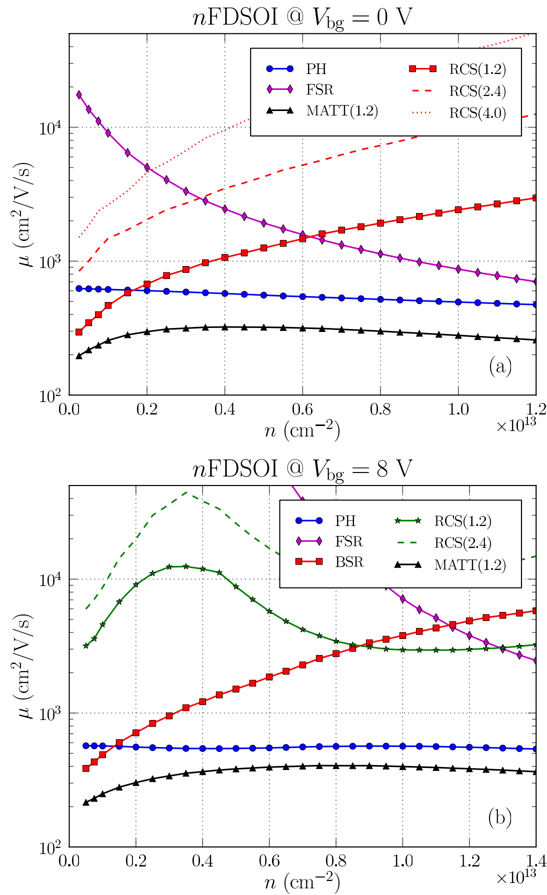

Fig. 4. Breakdown of the electron mobility in PH, FSR, BSR, and RCS components, at back gate voltages (a) $V_{bg} = 0$ V and (b) $V_{bg} = 8$ V. The PH, FSR, and BSR components are weakly dependent on t_{IL} (and are given for $t_{IL} = 2.4$ nm), while the RCS component is plotted for different ILs. BSR scattering is negligible at $V_{bg} = 0$ V and has not been plotted in (a) for the sake of clarity. The total mobility (MATT) of the $t_{IL} = 1.2$-nm device has been computed with Matthiessen's rule. It is close to the direct NEGF calculation shown in Fig. 1.

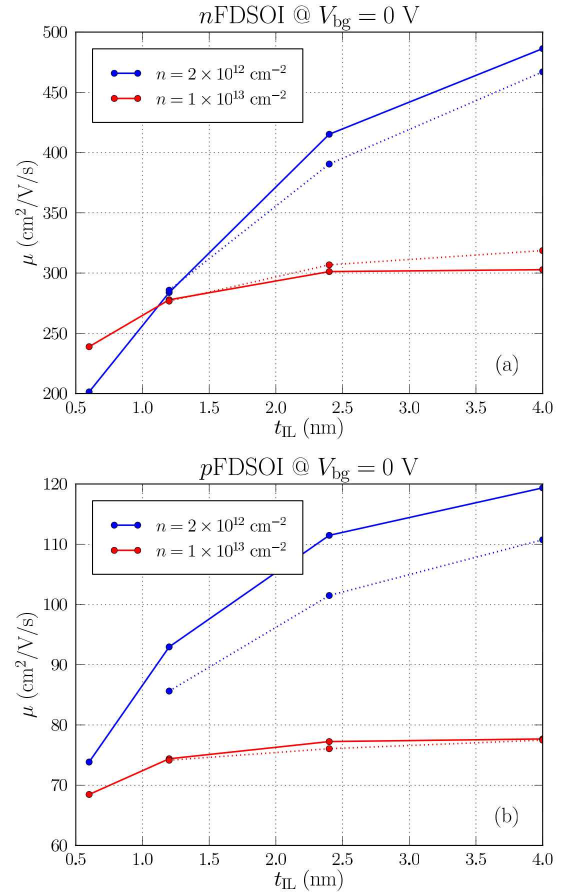

Fig. 5. Room-temperature (a) electron and (b) hole mobility as a function of t_{IL}, at two carrier densities $n = 2 \times 10^{12}$ cm^{-2} and $n = 1 \times 10^{13}$ cm^{-2}. The solid lines are the NEGF calculations, the dotted lines the experimental data.

The electron mobilities recomputed with these parameters are compared with experiment in Fig. 1. NEGF data extrapolated for $t_{IL} = 0.6$ nm (GO2) have been added to Fig. 1(a) to highlight trends down to very thin ILs (see later Section IV). NEGF reproduces the experimental data very well except possibly at large densities for $V_{bg} = 8$ V. The breakdown of the mobility in different components is plotted in Fig. 4 along with the result of Matthiessen's rule (2) for the 1.2-nm-thick IL. As discussed above, Matthiessen's rule holds surprisingly well (up to ≈10% for all ILs) using (1) as a definition of the partial mobility.

Figs. 1 and 4 give complementary insights into the physics and performances of these devices. The analysis of the carrier distribution in the film shows that inversion takes place at the front interface at $V_{bg} = 0$ V. The current at $V_{bg} = 0$ V is, therefore, essentially probing the quality of that interface, as in a conventional bulk MOSFET. Fig. 4(a) shows that scattering is actually dominated by phonons + RCS at low-carrier density, and by phonons + FSR at high-carrier density. The back interface roughness plays little role at zero or negative V_{bg} [and has not been plotted in Fig. 4(a)]. As expected, the RCS mobility increases with increasing density, as the remote charges get screened by the electron gas, while the FSR mobility decreases, as the electrons get confined closer to the interface by the effective field. Since the scattering strength of remote Coulomb charges increases (almost exponentially) with thinning the IL, the mobility at $V_{bg} = 0$ V is strongly dependent on t_{IL} at low-carrier density. However, in the thinnest ILs, RCS can significantly hinder the flow of electrons over the whole range of operation, as shown in Fig. 5(a).

The data at $V_{bg} = 8$ V bring additional information specific to FDSOI devices, and about electron–phonon interactions. As shown in Fig. 3 (but for holes), there is a transition between back interface inversion at low density to front interface inversion at high density. Consequently, scattering is dominated by phonons + BSR at low density, and by phonons + FSR at high density. The quality of the back interface can therefore also be probed in that regime. RCS plays a minor role at large back bias. Indeed, the electrons are either flowing very far from the front interface at low density, or screen the remote charges as they move to the front interface at high density. The interplay between the back to front interface transition (which strengthens RCS) and the screening (which weakens it) results in the complex behavior of the RCS mobility visible in Fig. 4(b). Interestingly, there is a range of densities around the peak mobility ($n \approx 9 \times 10^{12}$ cm^{-2}) where the mobility is mostly limited by electron–phonon interactions.

These devices therefore bring direct insights into the strength of these interactions. In particular, there is no doubt that the acoustic deformation potential needs to be increased around $D_{ac} = 15$ eV to reproduce the experimental data [6], [27]. Interestingly, the holes Ξ_{ac} must also be increased to match the experimental mobility, as discussed below.

We shall make a critical assessment of the structural parameters obtained with our procedure (3). These data suggest that the back interface is slightly better than the front interface, which might result from the complex gate-stack processing (oxide nitridation, high-κ, and TiN metal gate deposition). Our Δ_{FSR} and Δ_{BSR} are significantly smaller than those typically used in semiclassical KG solvers [16] (which would be closer to 0.5 nm), yet they are larger than most available AFM measurements (around 0.2 nm [26], [28], [29] on the top surface before processing). As discussed earlier, increasing the correlation length Λ around 2 nm or switching to a Gaussian autocorrelation function model [8] helps in reducing Δ_{FSR} and Δ_{BSR}, but has little impact (as we have verified on some test cases) on Figs. 1 and 4. As an example, using a Gaussian instead of an exponential auto-correlation function (with the same $\Lambda = 1.3$ nm) brings Δ_{FSR} and Δ_{BSR} in the $0.25 - 0.3$ nm range. As for RCS, the extracted n_{RCS} is quite large but in line with the literature [12], and provides an excellent description of the behavior of the mobility with t_{IL} [Fig. 5(a)]. Such a large n_{RCS} shall however, be responsible for a threshold voltage shift $\Delta V_t = -0.55$ V, which does not seem to be observed experimentally (although there are experimental uncertainties on some parameters controlling V_t). As discussed in [12], one possible solution to this dilemma is to assume a balanced distribution of positive and negative charges at the SiON/HfSiON interface or in the HfSiON itself. Further investigations are needed in that direction. In addition, we have neglected RPS in the front gate-stack [12], [13], whose description in NEGF is still challenging. Yet RPS is expected to make a significant contribution only in the thinnest ILs ($t_{IL} < 1$ nm) [12]. The marked loss of mobility predicted by NEGF in the 0.6-nm-thick IL (Fig. 1) might therefore be underestimated.

C. Holes

Holes shall provide a decisive test of the relevance of our description. The hole mobility at $V_{bg} = 0$ V and $V_{bg} = -8$ V is plotted in Fig. 2, and the breakdown of the mobility in PH, FSR, BSR, and RCS components is given in Fig. 6. As for electrons, the holes are essentially probing the front interface at $V_{bg} = 0$ V, while they switch from back to front interface at $V_{bg} = -8$ V (Fig. 3), and are therefore also probing the back interface.

It turns out that it is impossible to reproduce the experimental mobility (at any V_{bg}) without strengthening the hole–phonon interactions by about 80%. The data at $V_{bg} = -8$ V, where hole–phonon interactions are the very dominant mechanism, are a clear fingerprint of this trend. This can be achieved by increasing the acoustic deformation potential Ξ_{ac} from 10.2 to 15.5 eV. Although impressive, this enhancement is consistent with the case of electrons (D_{ac} from 9 to 14.6 eV).

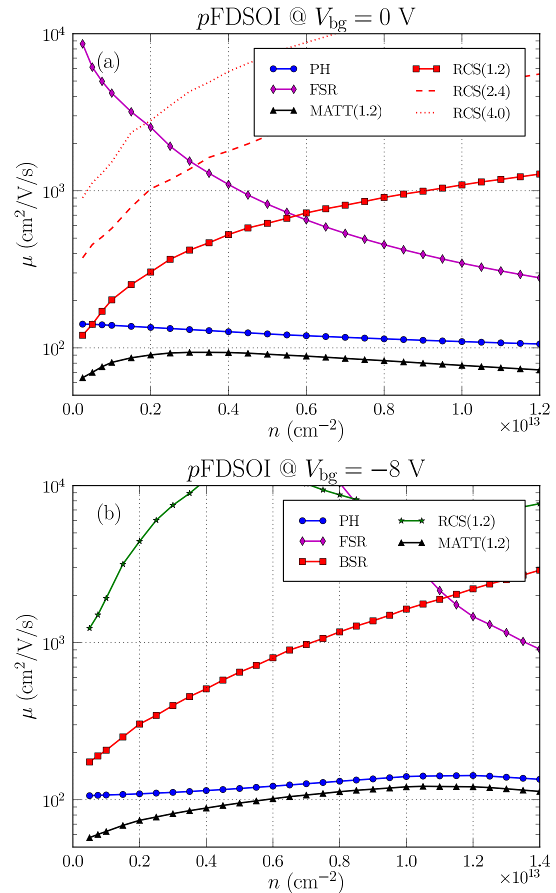

Fig. 6. Breakdown of the hole mobility in PH, FSR, BSR, and RCS components, at back gate voltages (a) $V_{bg} = 0$ V and (b) $V_{bg} = -8$ V. The PH, FSR, and BSR components are weakly dependent on t_{IL} (and are given for $t_{IL} = 2.4$ nm). The total mobility of the $t_{IL} = 1.2$-nm device has been computed with Matthiessen's rule (MATT). It is close to the direct NEGF calculation shown in Fig. 2.

With this change, we are able to reproduce the experimental data fairly well using the same structural parameters as for electrons (3).

The main discrepancies with experiment can be found at $V_{bg} = 0$ V. We lack scattering at low density [Fig. 5(b)], which might be corrected by slightly increasing n_{RCS}. We note, incidentally, that the dependence of the mobility on t_{IL} is much weaker for holes than for electrons (especially at negative V_{bg}), because RCS is outmatched by the strong hole–phonons interactions, and because the hole centroid is slightly farther from the top interface than the electron centroid at a given effective field. We can not rule out that n and p devices show different n_{RCS}. Yet, the mismatch between NEGF and experiment is not much larger than the 5% error bar we expect from the neglect of spin–orbit interactions.

Instead of increasing Ξ_{ac}, we might enhance both acoustic and optical deformation potentials in a similar way. The temperature dependence of the mobility is, however, slightly better in the former scenario (Fig. 7) than in the latter. Comparisons between NEGF and experiments [30] on trigate devices with 10×11 nm rectangular cross sections also suggest a similar enhancement of hole–phonons interactions.

The NEGF data for the phonon-limited hole mobility are in fair agreement with semiclassical KG calculations, as already

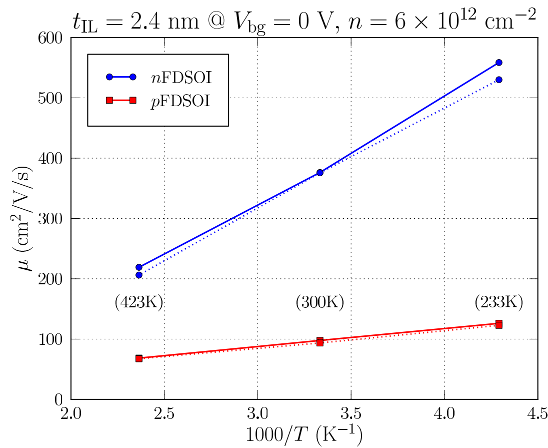

Fig. 7. Temperature dependence of the electron and hole mobilities in a FDSOI device with $t_{\rm IL} = 2.4$ nm at $V_{\rm bg} = 0$ V. The solid lines are the NEGF calculations, the dotted lines the experimental data (carrier density $n = 6 \times 10^{12}$ cm^{-2}).

shown for electrons [16]. This is however, not true for the other mechanisms, so that achieving a consistent description of electron and hole mobilities with the same structural parameters can be harder within KG [17]. NEGF is, in this respect, particularly attractive for holes, as it deals with their multibands character nonperturbatively.

It is unlikely that we are missing some scattering mechanism that we would have mistaken as an enhancement of carrier–phonons interactions. This mechanism shall be very strong, and have the same temperature and density dependence as carrier–phonons interactions. The microscopic details responsible for the enhancement of the electron– and hole–phonons interactions remain, however, unclear. While NEGF is very accurate for elastic mechanisms, the local, isotropic models used for carrier–phonons interactions are, admittedly, very simplified (but are the same as in most KG solvers). As mentioned in Section III, we have tried different models for the hole–phonons interactions (featuring nondiagonal, though still local self-energies), which all overestimate the phonon-limited mobility in the films by about 80% (using the same parameters as in bulk). To get a better insight into this problem, we are now attempting atomistic tight-binding calculations of the electron and hole mobility in thin films along the lines of [31] and [32]. These calculations, which account for all possible carrier–phonons interactions with a realistic phonon band structure, might provide the missing clues.

V. Conclusion

We have compared experimental electron and hole mobilities in UTBB-FDSOI devices with quantum calculations in the NEGF framework. Using a new methodology [16], we have reached a consistent description of electron and hole mobilities (same structural parameters) in agreement with the available experimental data. Furthermore, we have been able to break down the mobility into contributions from phonons, FSR and BSR, and RCS, in a way consistent with Matthiessen's rule. Our analysis shows or confirms that carrier–phonons interactions are strongly enhanced in thin films (with respect to bulk), although the underlying mechanisms are still unclear (but under investigation from an atomistic perspective). It also reveals the particular dependence of remote Coulomb scattering on the back gate bias, and its relative importance for electrons and holes. Finally, it demonstrates that back biasing is really a foremost tool to discriminate scattering mechanisms in thin films and can provide deep insight into the physics of FDSOI devices. Such calculations also show that quantum transport methods, such as NEGF, are now mature enough to handle realistic devices and provide valuable inputs for TCAD modeling. NEGF can, in particular, be used to extrapolate data and help clear the field for the next technology nodes, or to connect the low-temperature behavior of the devices (showing, e.g., fingerprints of localization on edge states or dopants) to their room-temperature characteristics [33].

References

[1] C. Fenouillet-Beranger *et al.*, "Fully-depleted SOI technology using high-*k* and single-metal gate for 32 nm node LSTP applications featuring 0.179μm^2 6T-SRAM bitcell," in *Proc. IEEE Int. Electron Devices Meeting (IEDM)*, Dec. 2007, pp. 267–270.

[2] C. Fenouillet-Beranger *et al.*, "FDSOI devices with thin BOX and ground plane integration for 32 nm node and below," *Solid-State Electron.*, vol. 53, no. 7, pp. 730–734, 2009.

[3] N. Planes *et al.*, "28nm FDSOI technology platform for high-speed low-voltage digital applications," in *Proc. Symp. VLSI Technol. (VLSIT)*, Jun. 2012, pp. 133–134.

[4] L. Ragnarsson *et al.*, "On the origin of the mobility reduction in bulk-Si, UTBOX-FDSOI and SiGe devices with ultrathin-EOT dielectrics," in *Proc. Int. Symp. VLSI Technol., Syst. Appl. (VLSI-TSA)*, Apr. 2011, pp. 1–2.

[5] A. Ohata *et al.*, "Impact of back-gate biasing on effective field and mobility in ultrathin silicon-on-insulator metal-oxide-semiconductor field-effect-transistors," *J. Appl. Phys.*, vol. 113, no. 14, pp. 144514-1–144514-8, 2013.

[6] D. Esseni, A. Abramo, L. Selmi, and E. Sangiorgi, "Physically based modeling of low field electron mobility in ultrathin single- and double-gate SOI n-MOSFETs," *IEEE Trans. Electron Devices*, vol. 50, no. 12, pp. 2445–2455, Dec. 2003.

[7] M. V. Fischetti, Z. Ren, P. M. Solomon, M. Yang, and K. Rim, "Six-band k·p calculation of the hole mobility in silicon inversion layers: Dependence on surface orientation, strain, and silicon thickness," *J. Appl. Phys.*, vol. 94, no. 2, pp. 1079–1095, 2003.

[8] S. M. Goodnick, D. K. Ferry, C. W. Wilmsen, Z. Liliental, D. Fathy, and O. L. Krivanek, "Surface roughness at the SI(100)-SIO_2 interface," *Phys. Rev. B*, vol. 32, no. 12, pp. 8171–8186, 1985.

[9] S. Jin, M. Fischetti, and T.-W. Tang, "Modeling of surface-roughness scattering in ultrathin-body SOI MOSFETs," *IEEE Trans. Electron Devices*, vol. 54, no. 9, pp. 2191–2203, Sep. 2007.

[10] F. Gamiz, J. B. Roldan, J. E. Carceller, and P. Cartujo, "Monte Carlo simulation of remote-Coulomb-scattering-limited mobility in metal–oxide–semiconductor transistors," *Appl. Phys. Lett.*, vol. 82, no. 19, pp. 3251–3253, 2003.

[11] M. Casse *et al.*, "Carrier transport in HfO_2/metal gate MOSFETs: Physical insight into critical parameters," *IEEE Trans. Electron Devices*, vol. 53, no. 4, pp. 759–768, Apr. 2006.

[12] P. Toniutti, P. Palestri, D. Esseni, F. Driussi, M. D. Michielis, and L. Selmi, "On the origin of the mobility reduction in n- and p-metal–oxide–semiconductor field effect transistors with hafnium-based/metal gate stacks," *J. Appl. Phys.*, vol. 112, no. 3, p. 034502, 2012.

[13] M. V. Fischetti, D. A. Neumayer, and E. A. Cartier, "Effective electron mobility in Si inversion layers in metal-oxide-semiconductor systems with a high-κ insulator: The role of remote phonon scattering," *J. Appl. Phys.*, vol. 90, no. 9, pp. 4587–4608, 2001.

[14] S. Reggiani, E. Gnani, A. Gnudi, M. Rudan, and G. Baccarani, "Low-field electron mobility model for ultrathin-body SOI and double-gate MOSFETs with extremely small silicon thicknesses," *IEEE Trans. Electron Devices*, vol. 54, no. 9, pp. 2204–2212, Sep. 2007.

[15] V.-H. Nguyen, F. Triozon, F. Bonnet, and Y.-M. Niquet, "Performances of strained nanowire devices: Ballistic versus scattering-limited currents," *IEEE Trans. Electron Devices*, vol. 60, no. 5, pp. 1506–1513, May 2013.

[16] Y.-M. Niquet, V.-H. Nguyen, F. Triozon, I. Duchemin, O. Nier, and D. Rideau, "Quantum calculations of the carrier mobility: Methodology, Matthiessen's rule, and comparison with semi-classical approaches," *J. Appl. Phys.*, vol. 115, no. 5, p. 054512, 2014.

[17] O. Nier *et al.*, "Multi-scale strategy for high-*k*/metal-gate UTBB-FDSOI devices modeling with emphasis on back bias impact on mobility," *J. Comput. Electron.*, vol. 12, no. 4, pp. 675–684, 2013.

[18] M. P. Anantram, M. S. Lundstrom, and D. E. Nikonov, "Modeling of nanoscale devices," *Proc. IEEE*, vol. 96, no. 9, pp. 1511–1550, Sep. 2008.

[19] V. Sverdlov, G. Karlowatz, S. Dhar, H. Kosina, and S. Selberherr, "Two-band k.p model for the conduction band in silicon: Impact of strain and confinement on band structure and mobility," *Solid-State Electron.*, vol. 52, no. 10, pp. 1563–1568, 2008.

[20] G. Bastard, *Wave Mechanics Applied to Semiconductor Heterostructures*. Les Ulis, France: Les Éditions de Physique, 1988.

[21] C. Jacoboni and L. Reggiani, "The Monte Carlo method for the solution of charge transport in semiconductors with applications to covalent materials," *Rev. Modern Phys.*, vol. 55, no. 3, pp. 645–705, 1983.

[22] J. Wang, E. Polizzi, and M. Lundstrom, "A three-dimensional quantum simulation of silicon nanowire transistors with the effective-mass approximation," *J. Appl. Phys.*, vol. 96, no. 4, pp. 2192–2203, 2004.

[23] (2014, Jun. 20). *The Calculations Were Run on the TGCC/Curie Machine*. [Online]. Available: http://www-hpc.cea.fr/en/complexe/tgcc-curie.htm

[24] F. Gámiz and J. B. Roldán, "Scattering of electrons in silicon inversion layers by remote surface roughness," *J. Appl. Phys.*, vol. 94, no. 1, pp. 392–399, 2003.

[25] D. Esseni and F. Driussi, "A quantitative error analysis of the mobility extraction according to the Matthiessen rule in advanced MOS transistors," *IEEE Trans. Electron Devices*, vol. 58, no. 8, pp. 2415–2422, Aug. 2011.

[26] A. Pirovano, A. Lacaita, G. Ghidini, and G. Tallarida, "On the correlation between surface roughness and inversion layer mobility in Si-MOSFETs," *IEEE Electron Device Lett.*, vol. 21, no. 1, pp. 34–36, Jan. 2000.

[27] T. Ohashi, T. Takahashi, N. Beppu, S. Oda, and K. Uchida, "Experimental evidence of increased deformation potential at MOS interface and its impact on characteristics of ETSOI FETs," in *Proc. IEEE Int. Electron Devices Meeting (IEDM)*, Dec. 2011, pp. 16.4.1–16.4.4.

[28] T. Yamanaka, S. J. Fang, H.-C. Lin, J. P. Snyder, and C. R. Helms, "Correlation between inversion layer mobility and surface roughness measured by AFM," *IEEE Electron Device Lett.*, vol. 17, no. 4, pp. 178–180, Apr. 1996.

[29] O. Bonno, S. Barraud, D. Mariolle, and F. Andrieu, "Effect of strain on the electron effective mobility in biaxially strained silicon inversion layers: An experimental and theoretical analysis via atomic force microscopy measurements and Kubo–Greenwood mobility calculations," *J. Appl. Phys.*, vol. 103, no. 6, p. 063715, 2008.

[30] R. Coquand *et al.*, "Scaling of high-κ/metal-gate TriGate SOI nanowire transistors down to 10 nm width," *Solid-State Electron.*, vol. 88, pp. 32–36, Oct. 2013.

[31] Y.-M. Niquet, C. Delerue, D. Rideau, and B. Videau, "Fully atomistic simulations of phonon-limited mobility of electrons and holes in $\langle 001\rangle$-, $\langle 110\rangle$-, and $\langle 111\rangle$-oriented Si nanowires," *IEEE Trans. Electron Devices*, vol. 59, no. 5, pp. 1480–1487, May 2012.

[32] W. Zhang, C. Delerue, Y.-M. Niquet, G. Allan, and E. Wang, "Atomistic modeling of electron-phonon coupling and transport properties in n-type [110] silicon nanowires," *Phys. Rev. B*, vol. 82, no. 11, p. 115319, 2010.

[33] B. Voisin *et al.*, "Few-electron edge-state quantum dots in a silicon nanowire field-effect transistor," *Nano Lett.*, vol. 14, no. 4, pp. 2094–2098, 2014.

Viet-Hung Nguyen received the M.S. degree in physics from the Institute of Physics, Hanoi, Vietnam, and the Hanoi National University of Education, Hanoi, in 2007, and the Ph.D. degree in physics from the University of Paris-Sud, Orsay, France, in 2010.

He has been a Researcher with the Institute of Physics (on leave) since 2010. He is currently with the Institut d'Électronique Fondamentale, Orsay.

Yann-Michel Niquet received the Engineering degree in electronics from the Institut Supérieur de l'Electronique et du Numérique, Lille, France, the master's degree in physics from the University of Paris-Sud, Orsay, France, in 1997, and the Ph.D. degree in physics from the University of Lille, Lille, in 2001.

He has been a permanent Researcher with the L Sim laboratory, INAC, CEA Grenoble, Grenoble, France, since 2003.

François Triozon received the M.S. degree in condensed matter physics from Ecole Normale Supérieure de Lyon, Lyon, France, in 1996, and the Ph.D. degree in physics from the University of Grenoble, Grenoble, France, in 2002.

He has been a permanent Researcher with LETI, CEA Grenoble, Grenoble, since 2005. He is involved in the modeling of the electronic transport of semiconductor and carbon nanostructures.

Ivan Duchemin received the Engineering degree in physics from the Institut National des Sciences Appliquées, Toulouse, France, in 2003, and the master's degree in nanosciences and the Ph.D. degree in physics from the Paul Sabatier University of Toulouse, Toulouse, in 2003 and 2006, respectively.

He has been a permanent Researcher with the L Sim laboratory, INAC, CEA Grenoble, Grenoble, France, since 2012.

Olivier Nier received the Engineering Degree from Polytech Grenoble, Grenoble, France, in 2011. He is currently pursuing the Ph.D. degree with STMicroelectronics, Crolles, France.

His current research interests include the modeling and simulation of nanoscales devices, in particular, the FDSOI technology.

Denis Rideau received the Ph.D. degree in physics from the University of Orsay, Orsay, France, in 2001, and the Engineering degree from the École Supérieure d'Ingénieurs en Électronique et Électrotechnique, Paris, France, in 1996.

He is currently involved in research and development in solid-state physics with STMicroelectronics, Crolles, France. He is also involved in RF modeling and the simulation of Si nanodevices.